Inorganic Chemistry

Article

Reaction Controlled Assemblies of Polyoxotungstates (-molybdates) and Coordination Polymers

Guangfeng Hou, Lihua Bi, Bao Li, and Lixin Wu*

State Key Laboratory of Supramolecular Structure and Materials, College of Chemistry, Jilin University, Changchun 130012, China

To investigate the influence of reaction conditions on the compound structures, five polyoxometalate (POM)-supported inorganic−organic hybrid compounds, $[Cu^I_3(L^1)_4][PW_{12}O_{40}]$ (**1**), $[Cu^I_3(L^1)_4][PMo_{12}O_{40}]$ (**2**), $[Cu^I_3(L^1)_4][PW_{12}O_{40}]$ (**3**), $[Cu^I_3(L^1)_3][PW_{12}O_{40}]$ (**4**), and $[Cu^I_3(L^2)_3][PMo_{12}O_{40}]$ (**5**) [L^1 = 1,4-bis(pyrazol-1-ylmethyl)benzene, L^2 = 4,4′-bis(pyrazol-1-ylmethyl)biphenyl], were hydrothermally synthesized by tuning the reactant species and molar ratio and reaction temperature and were characterized by elemental analysis, IR spectroscopy, PXRD, XPS, electrochemistry, SPS, and X-ray crystallography. Compounds **1** and **2** were synthesized in the isostructural state at 150 °C, in which L^1 ligands link Cu^I ions, generating a cationic 2D 6^3 (**hcb**) skeleton $\{[Cu_3(L^1)_4]^{3+}\}_n$-like sheet that further connects with POM anions, forming a neutral 2D (3,4)-connected network with a Schläfli symbol of $(5^3)_2(5^4;8^2)$. In contrast, compound **3** was synthesized at a relatively lower reaction temperature (130 °C) than that for the synthesis of **1** and **2**, which exhibits a similar 2D sheet-like cationic skeleton with **1** and **2**. Interestingly, the POM anions do not coordinate with the cationic moieties in **3**. Compounds **4** and **5** were synthesized with a relatively lower reactant molar ratio in comparison with that for the synthesis of **1**−**3**, in which the cationic coordination moieties all present 1D chain-like structures. Compound **4** exhibits a 3D (3,4)-connected **sqc74** framework with a Schläfli symbol of $(6;8^2)(6^4;8;10)$ formed by the POM anions linking $\{[Cu_3(L^1)_3]^{3+}\}_n$ cationic chains. In comparison to **4**, compound **5** shows a 3D supramolecular framework, which is formed by POM anions and $\{[Cu_3(L^2)_3]^{3+}\}_n$ cationic chains via hydrogen bonds. The structural difference of compounds **1**−**5** indicates that the reaction conditions perform a crucial influence on the structures of this series. The electrochemical properties of **2** and **5** and the SPS responses of **3**−**5** suggest that these compounds can be used as potential electrocatalytic or photocatalytic framework materials. In addition, EFISPS curves indicate that **3**−**5** possess the *n*-type semiconductor characteristic.

Introduction

The design and synthesis of inorganic−organic hybrid assemblies, for example, the construction of novel metal−organic frameworks (MOFs), have attracted considerable attention over recent years, because of both their intriguing architectures and properties as well as potential applications in catalysis, magnetism, and sensitive devices.[1,2] Generally, one effective approach for novel hybrid assemblies is the incorporation of functional building blocks, which can afford a synergic effect with MOFs. Polyoxometalates (POMs), as a unique class of inorganic metal oxide clusters with unmatched structural versatility,[3] abundant coordination sites,[4] and rich properties,[5] represent a significant type of inorganic building block for the construction of new MOF materials. To date, by introducing POMs into MOF systems, the obtained hybrid materials not only exhibit anticipated functional properties, for example, the improved surface area, dispersion degree and orientation of POMs, resulting

*To whom correspondence should be addressed. Tel.: (86)431-8516-8481. Fax: (86)431-8519-3421. E-mail: wulx@jlu.edu.cn.

(1) (a) Chae, H. K.; Siberio-Pérez, D. Y.; Kim, J.; Go, Y.; Eddaoudi, M.; Matzger, A. J.; O'Keeffe, M.; Yaghi, O. M. *Nature* **2004**, *427*, 523–527. (b) Eddaoudi, M.; Moler, D. B.; Li, H. L.; Chen, B. L.; Reineke, T. M.; O'Keeffe, M.; Yaghi, O. M. *Acc. Chem. Res.* **2001**, *34*, 319–330. (c) Battan, S. R.; Murray, K. S. *Coord. Chem. Rev.* **2003**, *246*, 103–130. (d) Millward, A. R.; Yaghi, O. M. *J. Am. Chem. Soc.* **2005**, *127*, 17998–17999. (e) Wong-Foy, A. G.; Matzger, A. J.; Yaghi, O. M. *J. Am. Chem. Soc.* **2006**, *128*, 3494–3495. (f) Lee, E. W.; Kim, Y. J.; Jung, D. Y. *Inorg. Chem.* **2002**, *41*, 501–506. (g) Lin, Z. Z.; Jiang, F. L.; Chen, L.; Yuan, D. Q.; Hong, M. C. *Inorg. Chem.* **2005**, *44*, 73–76.

(2) (a) Yaghi, O. M.; O'Keeffe, M.; Ockwig, N. W.; Chae, H. K.; Eddaoudi, M.; Kim, J. *Nature* **2003**, *423*, 705–714. (b) Rowsell, J. L. C.; Spencer, E. C.; Eckert, J.; Howard, J. A. K.; Yaghi, O. M. *Science* **2005**, *309*, 1350–1354. (c) Batten, S. R.; Robson, R. *Angew. Chem., Int. Ed.* **1998**, *37*, 1461–1494. (d) Carlucci, L.; Ciani, G.; Proserpio, D. M. *Coord. Chem. Rev.* **2003**, *246*, 247–289. (e) Andres, P. R.; Schubert, U. S. *Adv. Mater.* **2004**, *16*, 1043–1068.

(3) (a) Pope, M. T. *Heteropoly and Isopoly Oxometalates*; Springer Verlag: Berlin, 1983. (b) Long, D. L.; Burkholder, E.; Cronin, L. *Chem. Soc. Rev.* **2007**, *36*, 105–121. (c) Pradeep, C. P.; Long, D. L.; Streb, C.; Cronin, L. *J. Am. Chem. Soc.* **2008**, *130*, 14946–14947. (d) Fukaya, K.; Yamase, T. *Angew. Chem., Int. Ed.* **2003**, *42*, 654–658. (e) Zimmermann, M.; Belai, N.; Butcher, R. J.; Pope, M. T.; Chubarova, E. V.; Dickman, M. H.; Kortz, U. *Inorg. Chem.* **2007**, *46*, 1737–1740.

in enhanced performance such as catalytic efficiency,[6] but also reveal aesthetic topological structures.[7]

As a kind of typical structure in POM chemistry, due to size suitability and unity and structure stability, Keggin-type POMs have been mostly employed as structural units to construct POM-supported MOFs through linking with transition metals and organic ligands, which afford multidimensional topological architectures.[8] Most organic ligands are either rigid or flexible. As a typical rigid ligand, 4,4′-bipyridine was applied to react with transition metals and POMs, forming various POM-based rigid porous compounds,[9] where the pore size can be well controlled by changing POM anions. In contrast, flexible ligands are less used for the synthesis of POM-based coordination compounds. The limited report regards high dimensional POM-based coordination assemblies by using flexible 1,4-bis(1,2,4-triazol-1-yl)-butane ligand and its derivatives,[10] in which the flexible ligands allowed themselves to fit the coordination environ-ment of transition metal ions and POMs. However, the POM-supported MOFs based on those organic ligands combining rigidity and flexibility are rarely reported. Due to a rigid phenyl center linking two coordinated groups via flexible methylene sp^3-carbon atoms, the ligand 1,4-bis-(imidazol-1-ylmethyl)benzene (bix) and its analogue 1,4-bis-(1,2,4-triazol-1-ylmethyl)benzene (btx) were considered as this kind of ligand, providing a flexible feature with appropriate rigidity, as found in open structure or interpenetrating coordination polymers.[11,12] In addition, POM-supported MOFs based on these two ligands have revealed a high-dimensional coordination framework with novel topology.[13,14] It is of interest to see if similar ligands can lead to different topological structures through modified reaction conditions. With this motivation, we designed ligands 1,4-bis(pyrazol-1-ylmethyl)benzene (L^1) and 4,4′-bis(pyrazol-1-ylmethyl)-biphenyl (L^2) (see Scheme 1). Although the two ligands are similar to bix in structure, they have not yet been engaged in the synthesis of POM-based coordination compounds.

As expected, through the investigation of the influence of reaction conditions for the structures of compounds under hydrothermal conditions, five novel compounds were obtained, namely, $[Cu^I_3(L^1)_4][PW_{12}O_{40}]$ (**1**), $[Cu^I_3(L^1)_4][PMo_{12}O_{40}]$ (**2**), $[Cu^I_3(L^1)_4][PW_{12}O_{40}]$ (**3**), $[Cu^I_3(L^1)_3][PW_{12}O_{40}]$ (**4**), and $[Cu^I_3(L^2)_3][PMo_{12}O_{40}]$ (**5**) [L^1 = 1,4-bis(pyrazol-1-ylmethyl)benzene, L^2 = 4,4′-bis(pyrazol-1-ylmethyl)biphenyl]. To the best of our knowledge, these compounds represent the first examples of POM-based L^1 or L^2 coordination polymers. Compounds **1** and **2** are isostructural, exhibiting a 2D (3,4)-connected network with different POM anions, $[PW_{12}O_{40}]^{3-}$ (PW$_{12}$) for **1** and $[PMo_{12}O_{40}]^{3-}$ (PMo$_{12}$) for **2**, respectively. Compound **3** exhibits a 2D honeycomb network, in which PW$_{12}$ anions fill in the cavity of the cationic skeleton. Compound **4** exhibits a 3D (3,4)-connected **sqc74** framework,[15] constructed from PW$_{12}$ anions linking 1D cationic chains. And compound **5** is a hydrogen-bond-directed 3D supramolecular framework, in which each PMo$_{12}$ anion serves as a template arranged into six 1D cationic chains, forming a cubic cage around it. In addition to the crystal structures and spectral characteristics, the electrocatalysis of compounds **2** and **5** and the SPS and EFISPS of compounds **3**−**5** have been studied to lead to an understanding of their

(4) (a) Rodriguez-Albelo, L. M.; Ruiz-Salvador, A. R.; Sampieri, A.; Lewis, D. W.; Gómez, A.; Nohra, B.; Mialane, P.; Marrot, J.; Sécheresse, F.; Mellot-Draznieks, C.; Biboum, R. N.; Keita, B.; Nadjo, L.; Dolbecq, A. *J. Am. Chem. Soc.* **2009**, *131*, 16078–16087. (b) Bi, L. H.; Hou, G. F.; Wu, L. X.; Kortz, U. *CrystEngComm* **2009**, *11*, 1532–1535. (c) Bi, L. H.; Hou, G. F.; Li, B.; Wu, L. X.; Kortz, U. *Dalton Trans.* **2009**, 6345–6353. (d) Zheng, S. T.; Zhang, J.; Clemente-Juan, J. M.; Yuan, D. Q.; Yang, G. Y. *Angew. Chem., Int. Ed.* **2009**, *48*, 7176–7179. (e) Zheng, S. T.; Zhang, J.; Yang, G. Y. *Angew. Chem., Int. Ed.* **2008**, *47*, 3909–3913. (f) Anderson, T. M.; Neiwert, W. A.; Kirk, M. L.; Piccoli, P. M. B.; Schultz, A. J.; Koetzle, T., F.; Musaev, D. G.; Morokuma, K.; Cao, R.; Hill, C. L. *Science* **2004**, *306*, 2074–2077. (g) Fang, X.; Anderson, T. M.; Benelli, C.; Hill, C. L.—*Eur. J.* **2005**, *11*, 712–718. (h) Cao, R.; Anderson, T. M.; Hillesheim, D. A.; Kögerler, P.; Hardcastle, K. I.; Hill, C. L. *Angew. Chem., Int. Ed.* **2008**, *47*, 9380–9382.

(5) (a) Pope, M. T.; Müller, A. *Polyoxometalates: From Platonic Solids to Antiretroviral Activity*; Kluwer: Dordrecht, The Netherlands, 1994. (b) Pope, M. T.; Müller, A. *Polyoxometalates Chemistry: From Topology via Self-Assembly to Applications*; Kluwer: Dordrecht, The Netherlands, 2001. (c) Li, B.; Yan, Y.; Li, F. Y.; Xu, L.; Bi, L. H.; Wu, L. X. *Inorg. Chim. Acta* **2009**, *362*, 2796–2801. (d) Bi, L. H.; McCormac, T.; Beloshapkin, S.; Dempsey, E. *Electroanalysis* **2008**, *20*, 38–46. (e) Coronado, E.; Gómez-García, C. J. *Chem. Rev.* **1998**, *98*, 273–296. (f) Qi, W.; Wang, Y. Z.; Li, W.; Wu, L. X. *Chem.—Eur. J.* **2010**, *16*, 1068–1078. (g) Botar, B.; Geletii, Y. V.; Kögerler, P.; Musaev, D. G.; Morokuma, K.; Weinstock, I. A.; Hill, C. L. *J. Am. Chem. Soc.* **2006**, *128*, 1126–1127. (h) Geletii, Y. V.; Botar, B.; Kögerler, P.; Hillesheim, D. A.; Musaev, D. G.; Hill, C. L. *Angew. Chem., Int. Ed.* **2008**, *47*, 3896–3899.

(6) (a) Sun, C. Y.; Liu, S. X.; Liang, D. D.; Shao, K. Z.; Ren, Y. H.; Su, Z. M. *J. Am. Chem. Soc.* **2009**, *131*, 1883–1888. (b) Maksimchuk, N. V.; Timofeeva, M. N.; Melgunov, M. S.; Shmakov, A. N.; Chesalov, Y. A.; Dybtsev, D. N.; Fedin, V. P.; Kholdeeva, O. A. *J. Catal.* **2008**, *257*, 315–323. (c) Han, J. W.; Hill, C. L. *J. Am. Chem. Soc.* **2007**, *129*, 15094–15095.

(7) (a) Liu, C. M.; Zhang, D. Q.; Xiong, M.; Zhu, D. B. *Chem. Commun.* **2002**, 1416–1417. (b) Zhang, L. J.; Zhao, X. L.; Xu, J. Q.; Wang, T. G. *Datlon Trans* **2002**, 3275–3276. (c) Lan, Y. Q.; Li, S. L.; Wang, X. L.; Shao, K. Z.; Su, Z. M.; Wang, E. B. *Inorg. Chem.* **2008**, *47*, 529–534. (d) Fan, L. L.; Xiao, D. R.; Wang, E. B.; Li, Y. G.; Su, Z. M.; Wang, X. L.; Liu, J. *Cryst. Growth Des.* **2007**, *7*, 592–594. (e) Qi, Y. F.; Li, Y. G.; Qin, C.; Wang, E. B.; Jin, H.; Xiao, D. R.; Wang, X. L.; Chang, S. *Inorg. Chem.* **2007**, *46*, 3217–3130.

(8) (a) Yang, L.; Naruke, H.; Yamase, T. *Inorg. Chem. Commun.* **2003**, *6*, 1020–1024. (b) Reinoso, S.; Vitoria, P.; Gutiérrez-Zorrilla, J. M.; Lezama, L.; Madariage, J. M.; Felices, L. S.; Iturrospe, A. *Inorg. Chem.* **2007**, *46*, 4010–4021. (c) Felices, L. S.; Vitoria, P.; Gutiérrez-Zorrilla, J. M.; Reinoso, S.; Etxebarria, J.; Lezama, L. *Chem.—Eur. J.* **2004**, *10*, 5138–5146.

(9) (a) Wei, M. L.; He, C.; Hua, W. J.; Duan, C. Y.; Li, S. H.; Meng, Q. J. *J. Am. Chem. Soc.* **2006**, *128*, 13318–13319. (b) Inman, C.; Knaust, J. M.; Keller, S. *Chem. Commun.* **2002**, 156–157. (c) Kong, X. J.; Ren, Y. P.; Zheng, P. Q.; Long, Y. X.; Long, L. S.; Huang, R. B.; Zheng, L. S. *Inorg. Chem.* **2006**, *45*, 10702–10711. (d) Zhao, X. Y.; Liang, D. D.; Liu, S. X.; Sun, C. Y.; Cao, R. G.; Gao, C. Y.; Ren, Y. H.; Su, Z. M. *Inorg. Chem.* **2008**, *47*, 7133–7138.

(10) (a) Tian, A. X.; Ying, J.; Peng, J.; Sha, J. Q.; Pang, H. J.; Zhang, P. P.; Chen, M. Z.; Su, Z. M. *Inorg. Chem.* **2009**, *48*, 100–110. (b) Tian, A. X.; Ying, J.; Peng, J.; Sha, J. Q.; Han, Z. G.; Ma, J. F.; Su, Z. M.; Hu, N. H.; Jia, H. Q. *Inorg. Chem.* **2008**, *47*, 3274–3283. (c) Dong, B. X.; Peng, J.; Gómez-García, C. J.; Benmansour, S.; Jia, H. Q.; Hu, N. H. *Inorg. Chem.* **2007**, *46*, 5933–5941.

(11) (a) Meng, X. R.; Song, Y. L.; Hou, H. W.; Han, H. Y.; Xiao, B.; Fan, Y. T.; Zhu, Y. *Inorg. Chem.* **2004**, *43*, 3528–3536. (b) Meng, X. R.; Liu, Y. R.; Song, Y. L.; Hou, H. W.; Fan, Y. T.; Zhu, Y. *Inorg. Chim. Acta* **2005**, *358*, 3024–3032.

(12) (a) Hoskins, B. F.; Robson, R.; Slizys, D. A. *J. Am. Chem. Soc.* **1997**, *119*, 2952–2953. (b) Hoskins, B. F.; Robson, R.; Slizys, D. A. *Angew. Chem., Int. Ed. Engl.* **1997**, *36*, 2336–2338. (c) Carlucci, L.; Ciani, G.; Proserpio, D. M. *Cryst. Growth Des.* **2005**, *5*, 37–39. (d) Zhang, L.; Lü, X. Q.; Chen, C. L.; Tan, H. Y.; Zhang, H. X.; Kang, B. S. *Cryst. Growth Des.* **2005**, *5*, 283–287. (e) Zhu, H. F.; Fan, J.; Okamura, T. A.; Sun, W. Y.; Ueyama, N. *Cryst. Growth Des.* **2005**, *5*, 289–294.

(13) (a) Qin, C.; Wang, X. L.; Yuan, L.; Wang, E. B. *Cryst. Growth Des.* **2008**, *8*, 2093–2095. (b) Zhang, P. P.; Peng, J.; Sha, J. Q.; Tian, A. X.; Pang, H. J.; Chen, Y.; Zhang, M. *CrystEngComm* **2009**, *11*, 902–908. (c) Qin, C.; Wang, X. L.; Wang, E. B.; Su, Z. M. *Inorg. Chem.* **2008**, *47*, 5555–5557. (d) Dong, B. X.; Xu, Q. *Cryst. Growth Des.* **2009**, *9*, 2776–2782.

(14) (a) Meng, J. X.; Lu, Y.; Li, Y. G.; Fu, H.; Wang, E. B. *Cryst. Growth Des.* **2009**, *9*, 4116–4126. (b) Dong, B. X.; Xu, Q. *Inorg. Chem.* **2009**, *48*, 5861–5873.

(15) (a) Ramsden, S. J.; Robins, V.; Hyde, S. T.; Hungerford, S. *EPINET: Euclidean Patterns in Non-Euclidean Tilings*; The Australian National University: Canberra, Australia, 2005−2009; http://epinet.anu.edu.au/ (accessed Jun 2010). (b) Ramsden, S. J.; Robins, V.; Hyde, S. T. *Acta Crystallogr., Sect. A* **2009**, *65*, 81–108.

Scheme 1. Schematic Representation of 1,4-Bis(pyrazol-1-ylmethyl)-benzene (L^1) and 4,4′-Bis(pyrazol-1-ylmethyl)biphenyl (L^2)
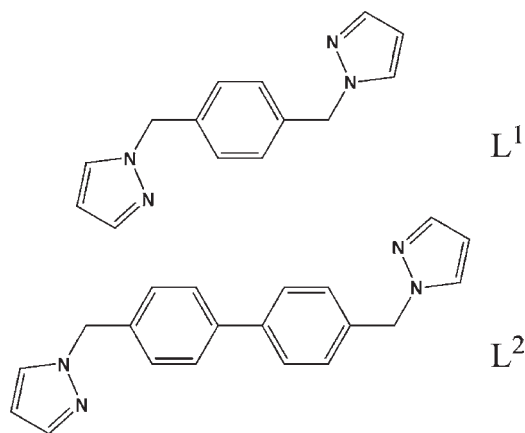
functional properties. According to present thought, on one hand, we obtained novel POM-supported MOFs, while on the other hand, we developed a deep understanding of ligand geometry and reaction conditions on POM-supported MOFs.

Experimental Section

Materials and General Methods. All commercially available chemicals were of reagent grade and used as received without further purification. The ligands 1,4-bis(pyrazol-1-ylmethyl)-benzene (L^1)[12a] and 4,4′-bis(pyrazol-1-ylmethyl)biphenyl (L^2)[16] were prepared according to the literature procedures.

Elemental analyses of C, H, and N were performed on a Perkin-Elmer 2400 CHN elemental analyzer. The IR spectra were recorded on a Bruker IFS 66v FT-IR spectrometer equipped with a DGTS detector (32 scans) using KBr pellets. Powder X-ray diffraction (PXRD) data were collected with Cu Kα (λ = 1.542 Å) radiation on a Rigaku D/Max-2500 X-ray diffractometer. X-ray photoelectron spectroscopy (XPS) analyses were performed on a VG Escalab 250 spectrometer with an Al Kα (1486.5 eV) achromatic X-ray source. Surface photo-voltage spectroscopy (SPS) and electric field-induced SPS (EFISPS) were carried out on a self-made instrument equipped with a Xenon lamp of 500 W, precision monochromators, a SR-830 Lock-in amplifier, a chopper, and a computer. Electro-chemical measurements were carried out on CHI 660C electro-chemical workstation at room temperature under a nitrogen atmosphere. A three electrode electrochemical cell was used with a modified glassy carbon electrode (GCE) as the working electrode, a platinum wire as the counter, and a Ag/AgCl as the reference electrode. The working electrode was prepared as follows: compound **2** or **5** (5 mg) was dissolved in 2 mL of acetonitrile solution under ultrasonic conditions to give a clear solution. The resulting solution was dropped onto the surface of the GCE and dried in the air. This was repeated until a uniform film on the GCE surface was obtained. This modified GCE can be used as the working electrode.

Synthesis of $[Cu^I_3(L^1)_4][PW_{12}O_{40}]$ (1). A mixture of Na$_2$-WO$_4$·2H$_2$O (0.66 g, 2.0 mmol), L^1 (0.19 g, 0.8 mmol), and Cu(NO$_3$)$_2$·3H$_2$O (0.19 g, 0.8 mmol) was dissolved in 15 mL of distilled water at room temperature, and then four drops of phosphoric acid were added to the above solution. When the pH value of the mixture was adjusted to about 1.7−2.2 with 4.0 M HCl, the suspension was sealed in a 25 mL Teflon-lined autoclave and heated at 150 °C for 5 days. After slow cooling to room temperature, red-brown rodlike crystals were filtered and

(16) Fei, B. L.; Sun, W. Y.; Zhang, Y. A.; Yu, K. B.; Tang, W. X. *J. Chem. Soc., Dalton Trans.* **2000**, 2345–2348.

washed with distilled water (43% yield based on W). Elemental Analysis Calcd. for C$_{56}$H$_{56}$N$_{16}$Cu$_3$PW$_{12}$O$_{40}$: C, 16.73; H, 1.40; N, 5.57. Found: C, 16.78; H, 1.46; N, 5.38. IR (KBr, cm^{-1}): 3116 (w), 1515 (w), 1423 (m), 1407 (m), 1275 (w), 1078 (m), 964 (s), 885 (s), 816 (s), 758 (s), 613 (w), 515 (m), 444 (m).

Synthesis of $[Cu^I_3(L^1)_4][PMo_{12}O_{40}]$ (2). The preparation of compound **2** was similar to that of **1** except that Na$_2$MoO$_4$·2H$_2$O (0.48 g, 2 mmol) was used instead of Na$_2$WO$_4$·2H$_2$O. Red-brown block crystals were filtered and washed with distilled water (50% yield based on Mo). Elemental Analysis Calcd. for C$_{56}$H$_{56}$N$_{16}$Cu$_3$PMo$_{12}$O$_{40}$: C, 22.68; H, 1.90; N, 7.56. Found: C, 22.81; H, 1.97; N, 7.42. IR (KBr, cm^{-1}): 3122 (w), 2927 (w), 1626 (w), 1517 (m), 1423 (m), 1405 (m), 1280 (w), 1063 (m), 958 (s), 880 (m), 808 (s), 754 (s), 611 (w), 505 (w).

Synthesis of $[Cu^I_3(L^1)_4][PW_{12}O_{40}]$ (3). The preparation of compound **3** was similar to that of **1** except that the autoclave was heated at 130 °C instead of 150 °C. Red-brown block crystals were filtered and washed with distilled water (47% yield based on W). Elemental Analysis Calcd. for C$_{56}$H$_{56}$N$_{16}$Cu$_3$P-W$_{12}$O$_{40}$: C, 16.73; H, 1.40; N, 5.57. Found: C, 16.57; H, 1.36; N, 5.49. IR (KBr, cm^{-1}): 3126 (w), 1519 (w), 1423 (w), 1406 (m), 1352 (w), 1272 (w), 1079 (m), 978 (s), 891 (m), 816 (s), 764 (s), 611 (w), 515 (m), 442 (m).

Synthesis of $[Cu^I_3(L^1)_3][PW_{12}O_{40}]$ (4). The preparation of compound **4** was similar to that of **3** except that the quantities of L^1 and Cu(NO$_3$)$_2$·3H$_2$O were changed from 0.8 mmol and 0.19 g to 0.4 mmol and 0.10 g, respectively. Yellow-brown block crystals were filtered and washed with distilled water (45% yield based on W). Elemental Analysis Calcd. for C$_{42}$H$_{42}$N$_{12}$Cu$_3$P-W$_{12}$O$_{40}$: C, 13.34; H, 1.12; N, 4.44. Found: C, 13.27; H, 1.08; N, 4.55. IR (KBr, cm^{-1}): 3116 (w), 1519 (w), 1421 (m), 1408 (m), 1271 (w), 1080 (m), 978 (s), 893 (m), 814 (s), 756 (m), 609 (w), 514 (w).

Synthesis of $[Cu^I_3(L^2)_3][PMo_{12}O_{40}]$ (5). The preparation of compound **5** was similar to that of **4** except that Na$_2$MoO$_4$·2H$_2$O (0.48 g, 2 mmol) and L^2 (0.12 g, 0.4 mmol) were used instead of Na$_2$WO$_4$·2H$_2$O and L^1, respectively. Red-brown block crystals were filtered and washed with distilled water (55% yield based on Mo). Elemental Analysis Calcd. for C$_{60}$-H$_{54}$N$_{12}$Cu$_3$PMo$_{12}$O$_{40}$: C, 24.38; H, 1.84; N, 5.69. Found: C, 24.29; H, 1.76; N, 5.75. IR (KBr, cm^{-1}): 3124 (w), 2973 (w), 2922 (w), 1633 (w), 1520 (w), 1420 (w), 1404 (m), 1277 (w), 1061 (s), 958 (s), 879 (m), 804 (s), 754 (m), 604 (w), 503 (w).

X-Ray Crystallography. Single-crystal X-ray diffraction data for compounds **1**−**5** were collected on a Rigaku R-AXIS RAPID imaging plate diffractometer with graphite-monochro-mated Mo Kα (λ = 0.71073 Å) at 293K. Empirical absorption corrections based on equivalent reflections were applied. The structures of **1**−**5** were solved by direct methods and refined by full-matrix least-squares methods on F^2 using the SHELXS-97 crystallographic software package.[17,18] All non-hydrogen atoms were refined anisotropically. The hydrogen atoms of the L^1 and L^2 molecules were placed in calculated positions and treated as riding on their parents. The Cu1 atom in compound **3** is disordered into two positions, and each position has a site occupancy factor of 0.5. In addition, the phosphate centers of the POMs in **1**−**5** are all disordered. The crystal parameters, data collection, and refinement results for **1**−**5** are summarized in Table 1. Selected bond lengths and angles are listed in Table S1 (see the Supporting Information). Crystallography data have been deposited to the Cambridge Crystallography Data Centre with deposition numbers CCDC: 729896, 734415, 735475, 732393, and 734595 for **1**−**5**, respectively.

(17) Sheldrick, G. M. *SHELXS-97*; University of Göttingen: Göttingen, Germany, 1997.

(18) Sheldrick, G. M. *SHELXL-97*; University of Göttingen: Göttingen, Germany, 1997.

Table 1. Crystal Data and Structure Refinements for Compounds **1–5**

	1	**2**	**3**	**4**	**5**
empirical formula	$C_{56}H_{56}N_{16}Cu_3$-$PW_{12}O_{40}$	$C_{56}H_{56}N_{16}Cu_3$-$PMo_{12}O_{40}$	$C_{56}H_{56}N_{16}Cu_3$-$PW_{12}O_{40}$	$C_{42}H_{42}N_{12}Cu_3$-$PW_{12}O_{40}$	$C_{60}H_{54}N_{12}Cu_3$-$PMo_{12}O_{40}$
fw	4020.96	2966.04	4020.96	3782.58	2956.05
cryst syst	triclinic	triclinic	triclinic	triclinic	cubic
space group	$P\bar{1}$	$P\bar{1}$	$P\bar{1}$	$P\bar{1}$	$Ia\bar{3}$
a (Å)	11.443(1)	11.453(4)	11.073(4)	12.029(6)	32.631(4)
b (Å)	14.144(1)	14.185(7)	13.660(4)	12.671(5)	32.631(4)
c (Å)	15.401(2)	15.336(5)	15.848(4)	13.429(5)	32.631(4)
α (deg)	111.463(2)	111.290(16)	114.410(9)	102.340(15)	90
β (deg)	97.523(2)	97.970(14)	90.010(12)	109.300(16)	90
γ (deg)	109.784(1)	110.110(15)	106.630(13)	105.490(17)	90
V (Å^3)	2088.5(4)	2078.7(14)	2072.2(11)	1756.0(13)	34745(7)
Z	1	1	1	1	16
D_{calc} (g cm^{-3})	3.197	2.369	3.222	3.577	2.260
μ(mm^{-1})	17.307	2.609	17.443	20.569	2.496
F(000)	1814	1430	1814	1687	22773
reflns collected/ unique	11942/7361	16036/7207	15737/7004	13125/5858	126608/4995
R(int)	0.0212	0.0200	0.0525	0.0872	0.0693
GOF on F^2	1.101	1.020	1.270	1.094	1.186
$R_1{}^a$ [$I > 2\sigma(I)$]	0.0373	0.0466	0.0677	0.0619	0.0481
wR_2 [$I > 2\sigma(I)$]	0.0787	0.0967	0.1551	0.1274	0.1246
$R_1{}^a$ (all)	0.0479	0.0526	0.0720	0.0704	0.0605
$wR_2{}^b$ (all)	0.0837	0.0997	0.1570	0.1317	0.1309

$^a R_1 = \sum ||F_o| - |F_c||/\sum |F_o|$. $^b wR_2 = \{\sum [w(F_o{}^2 - F_c{}^2)^2/\sum w(F_o{}^2)^2]\}^{1/2}$.

Results and Discussion

Hydrothermal methods are widely used in the synthesis of inorganic−organic hybrid compounds based on POMs, because under such reaction conditions, the problems of reactants' solubility can be solved. As well-known, in the hydrothermal reaction many factors can affect the structures or components of compounds. For this purpose, we investigate the influence of reaction temperature, reactant species, and reactant molar ratio on the compound structures.

In addition, in compounds **1–5**, the oxidation state of Cu ions can be definitely assigned as +1 on the basis of the bond XPS, bond valence sum calculations,[19] coordination environments, and crystal color, which may be a result of the reduction of the N-containing L^1 or L^2 ligand toward Cu^{2+} ions; similar phenomena have been reported in the previous publications.[14b,20] In the POM building blocks of **1–5**, the center [PO_4] moieties are observed to be disordered similar to the previous reports,[21] and all W and Mo atoms are in +6 oxidation state confirmed by the XPS.

Crystal Structure Description. **[$Cu^I_3(L^1)_4(PW_{12}O_{40})$] (1) and [$Cu^I_3(L^1)_4(PMo_{12}O_{40})$] (2).** Single-crystal X-ray diffraction analysis shows that compounds **1** and **2** are isostructural, so only the structure of **1** is described here in detail. Compound **1** crystallizes in the triclinic system with the $P\bar{1}$ space group. As shown in Figure 1a, there are two crystallographically independent Cu^I ions, in which the Cu1 ion lies on a symmetry center and the Cu1 ion is four-coordinated in a parallelogram geometry environment formed by two N atoms from two L^1 molecules and

two O atoms from two PW_{12} anions with bond distances of 1.89(1) Å (Cu1−N1) and 2.60(1) Å (Cu1−O12). The *cis* bond angles centered at the Cu1 ion are close to 90° (in the range of 89.6(3)−90.4(3)°), and *trans* bond angles are equal to 180°. The Cu2 ion is three-coordinated in a distorted Y-type geometry environment, coordinated by three N atoms from three L^1 molecules. The bond distances and angles around Cu2 are 1.93(1)−2.04(1) Å for Cu2−N and 102.4(4)−142.5(4)° for N−Cu2−N.

In **1**, the L^1 molecules exhibit both a C-shaped conformation with two pyrazole rings extending to one side of the benzene ring and a Z-shaped conformation with two pyrazole rings extending to opposite sides of the benzene ring, which bridge the Cu^I ions to form a cationic 2D 6^3 (**hcb**) skeleton. As shown in Figure 1b, four C-shaped L^1 molecules (in the vertical direction) and four Z-shaped L^1 molecules (in the horizontal direction) coordinate with eight Cu^I ions, forming an octagonal cavity with dimensions of ca. 14.8 × 18.2 Å. Furthermore, the PW_{12} cluster acts as a bidentate linker bridging the Cu^I ions via the terminal O atoms of PW_{12} to form infinite straight POM anion-based chains (Figure 1c). These POM anion chains graft onto the cationic skeletons by sharing the Cu1 ions giving rise to a POM containing a neutral 2D (3,4)-connected network with a Schläfli symbol of $(5^3)_2(5^4;8^2)$ (Figure 1d). Adjacent networks are stacked in an A−B type offset fashion and linked by C−H···O hydrogen bonds into a 3D supramolecular framework (Figure 1e; for hydrogen bond distances and angles, see Table S2, Supporting Information).

[$Cu^I_3(L^1)_4(PW_{12}O_{40})$] (3). It is interesting that when the reaction temperature is changed from 150 to 130 °C, compound **3** displays some difference in unit cell parameters and the coordination geometry with **1**. Single-crystal X-ray diffraction analysis shows that compound **3** also belongs to the triclinic system with the $P\bar{1}$ space group. In comparison with **1**, the unit cell parameters of **3** are similar in length and somewhat different in angles (Table 1).

(19) Brown, I. D.; Altermatt, D. *Acta Crystallogr., Sect. B* **1985**, *41*, 244–247.

(20) (a) Hagrman, D.; Zubieta, C.; Rose, D. J.; Zubieta, J.; Haushalter, R. C. *Angew. Chem., Int. Ed. Engl.* **1997**, *36*, 873–875. (b) Hagrman, D.; Zapf, P. J.; Zubieta, J. *J. Chem. Soc., Chem. Commun.* **1998**, 1283–1824. (c) Lu, C. Z.; Wu, C. D.; Zhuang, H. H.; Huang, J. S. *Chem. Mater.* **2002**, *14*, 2649–2655. (d) Lu, Y.; Xu, Y.; Wang, E. B.; Lü, J.; Hu, C. W.; Xu, L. *Cryst. Growth Des.* **2005**, *5*, 257–260.

(21) Han, Z. G.; Gao, Y. Z.; Zhai, X. L.; Peng, J.; Tian, A. X.; Zhao, Y. L.; Hu, C. W. *Cryst. Growth Des.* **2009**, *5*, 1225–1234.
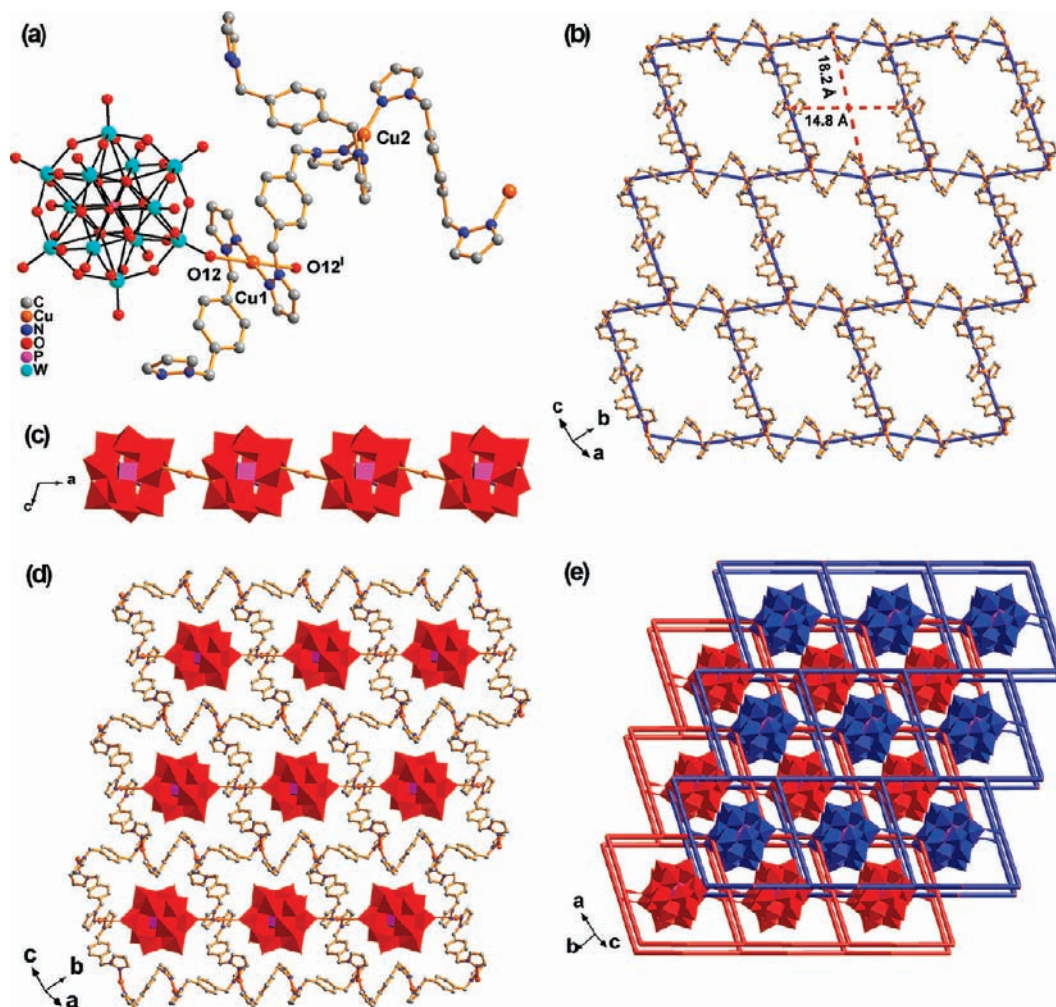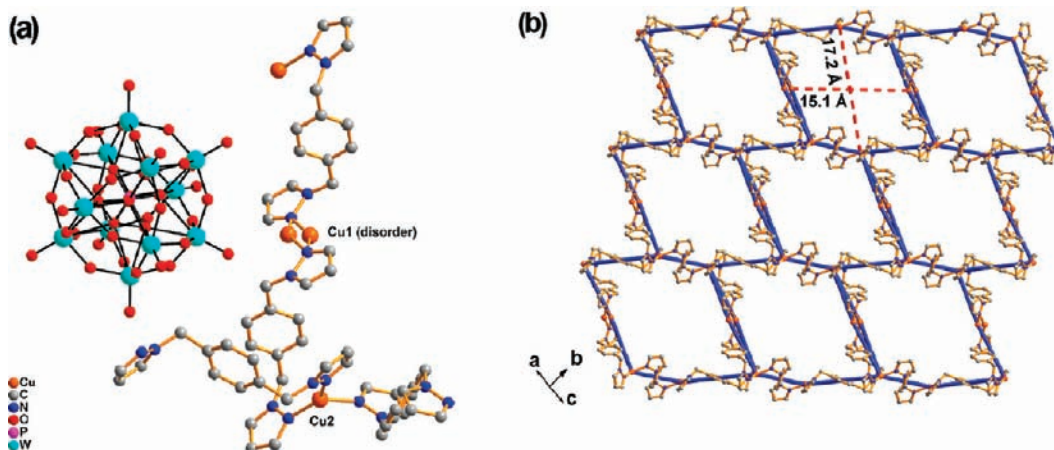
Figure 1. (a) Ball-and-stick representation of the asymmetric unit of **1**, where hydrogen atoms are omitted for clarity. (b) 2D 6^3 (**hcb**) coordination network with a cavity of 14.8×18.2 Å. (c) 1D polyhedral coordination chain of PW_{12} anions. (d) View of POM containing a neutral 2D (3,4)-connected network with a Schläfli symbol of $(5^3)_2(5^4;8^2)$. (e) Schematic illustration of A–B type stacking framework. Symmetry code: (I) $-x$, $1-y$, $2-z$.

As shown in Figure 2a, there are two crystallographically independent Cu^I ions, in which Cu1 is disordered. The Cu1 ion is two-coordinated in a linear geometry environment, coordinated by two N atoms from two L^1 molecules with a bond distance of 2.19(3) Å (Cu1–N1) and a bond angle of 151.5(7)°. The Cu2 ion is three-coordinated in a Y-type geometry environment with bond distances of 1.96(2)–2.10(2) Å and bond angles of 110.3(7)–137.0(7)°.

Interestingly, we observed that there is an intermediate state of the C-shaped and Z-shaped configuration of the L^1 molecule (Figure S1, Supporting Information). The coordination network in **3** is built up by four Z-shaped and four intermediate states of L^1 molecules, in which an eight-nuclear cavity is observed with dimensions of ca. 15.1×17.2 Å (Figure 2b). In contrast to **1**, the nearest distance between the Cu1 ion and PW_{12} moiety of **3** is 2.91(1) Å, indicating that the inserted PW_{12} anion is only stabilized by hydrogen bonds, which differ from the coordination interactions in **1** (Figure S2, Supporting Information). Finally, a hydrogen-bond-stabilized 3D supramolecular framework is found similar to **1** (for hydrogen bond distances and angles, see Table S2, Supporting Information).

$[Cu^I_3(L^1)_3(PW_{12}O_{40})]$ (**4**). In order to evaluate the influence of the reactant molar ratio on the construction of the products, compared with **3**, half the amounts of L^1 and $Cu(NO_3)_2\cdot 3H_2O$ are used to synthesize compound **4**. Single-crystal X-ray diffraction analysis shows that compound **4** also crystallizes in the triclinic system with the $P\bar{1}$ space group. Compound **4** consists of three L^1 molecules, three Cu^I ions, and one PW_{12} anion, which lack one L^1 molecule in relation to **3**. There are two kinds of crystallographically unique Cu ions. The Cu1 ion shows a T-type geometry by two N atoms from two L^1 ligands and one O atom of the PW_{12} anion. The bond distances and angles around the Cu1 ion are 1.86(2) and 1.87(2) Å for Cu1–N, 2.64(2) Å for Cu1–O, 175.0(7)° for N–Cu1–N, and 95.8(8) and 85.9(6)° for N–Cu1–O. The Cu2 ion is two-coordinated in a linear geometry by two N atoms from two L^1 ligands. The bond distances and angles around the Cu2 ion are 1.87(2) Å and 180.0(1)°. The weak Cu–O interactions are found with distances of 2.82(1) Å in **4** (Figure 3a).

In **4**, the L^1 molecules exhibit both the Z-shaped conformation and the intermediate state of the C/Z-shaped conformation as in **3**, which bridge the Cu^I ions to form a 1D cationic chain (Figure S3, Supporting Information). The PW_{12} anions act as bidentate linkers

Figure 2. (a) Ball-and-stick representation of the asymmetric unit of **3**. Hydrogen atoms are omitted for clarity. (b) 2D 6^3 (**hcb**) coordination network with a cavity of 15.1 × 17.2 Å.
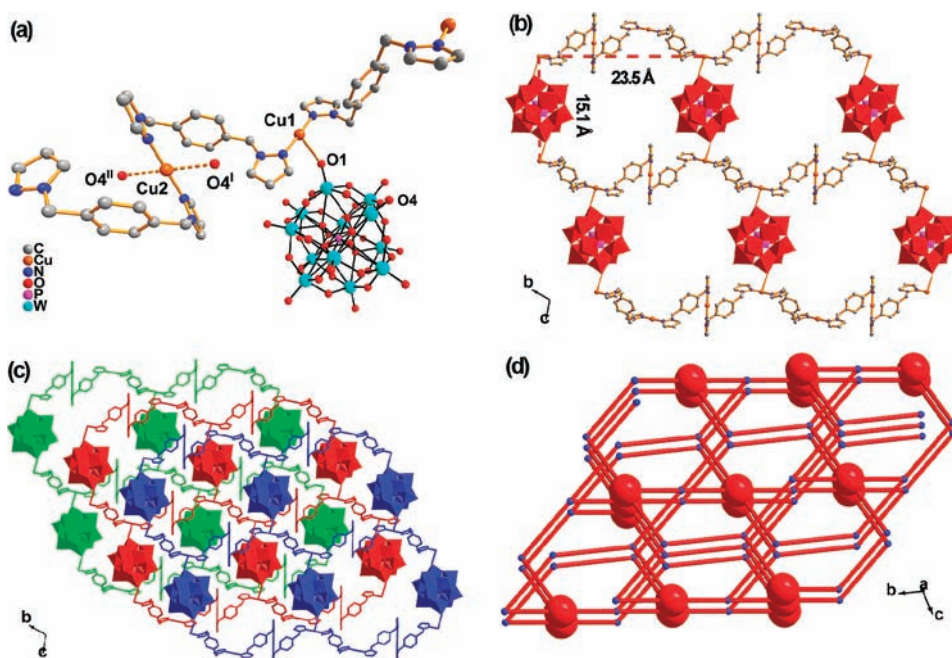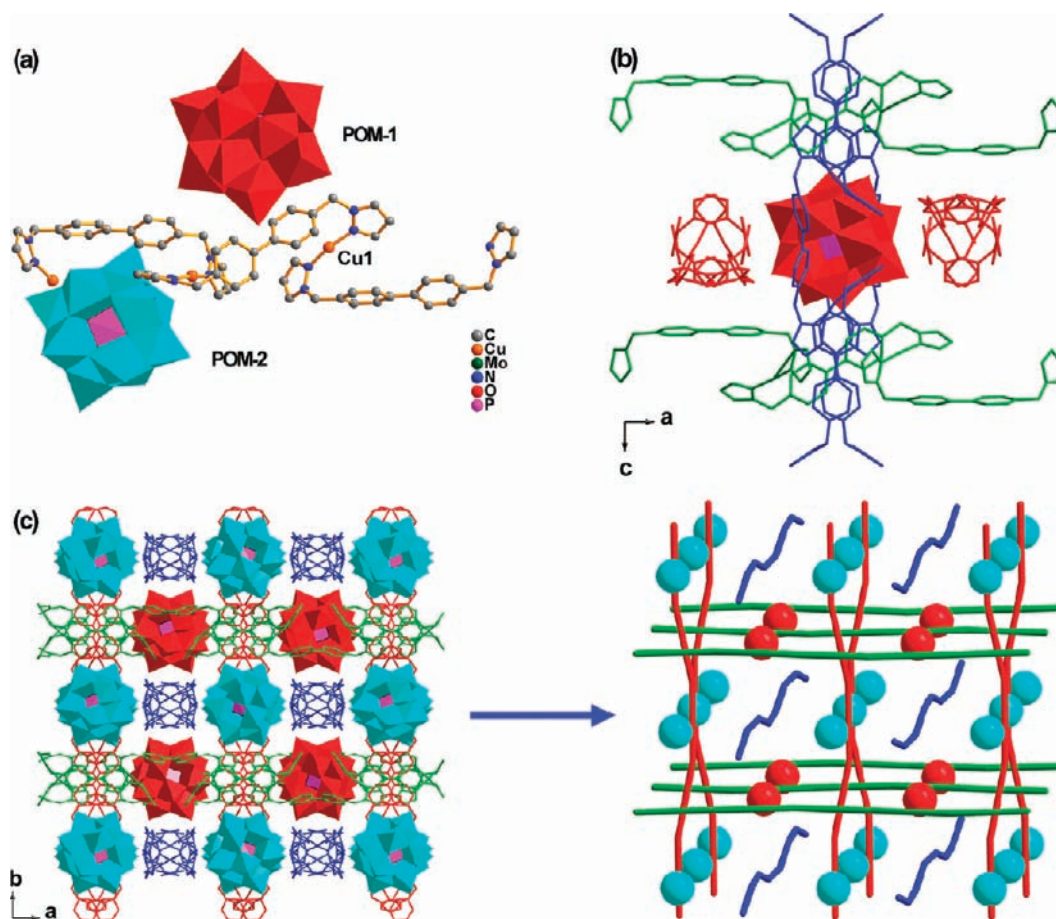

Figure 3. (a) Ball-and-stick representation of the asymmetric unit of **4**, in which the dashed line indicates a weak Cu−O interaction and hydrogen atoms are omitted for clarity. (b) View of the 2D net constructed of PW_{12} and $\{[Cu_3(L^1)_3]^{3+}\}_n$ moieties. (c) Illustration of A−B−C type stacking networks. (d) Schematic illustration of 3D (3,4)-connected **sqc74** framework with a Schläfli symbol of $(6;8^2)(6^4;8;10)$. Color code: a red ball denotes PW_{12}, and a blue ball represents a Cu^I ion. Symmetry codes: (I) $1 − x, 1 − y, 1 − z$; (II) $1 + x, 1 + y, 1 + z$.

bridging these coordination chains also to form a 2D honeycomb network but with a larger cavity of 23.5 × 15.1 Å (Figure 3b). Interestingly, these neutral sheets are stacked in an A−B−C type with an offset fashion that is different from the A−B type in **1**−**3** (Figure 3c). Furthermore, when the weak Cu−O interactions between the adjacent layers are considered, one 3D (3,4)-connected **sqc74** framework would be built up with a Schläfli symbol of $(6;8^2)(6^4;8;10)$ (Figure 3d, Figure S4, Supporting Information).

$[Cu^I_3(L^2)_3(PMo_{12}O_{40})]$ (**5**). Finally, in order to evaluate the influence of the ligand on the construction of the products, the L^2 molecule with a longer rigid spacer was used to synthesize compound **5**. Single-crystal X-ray diffraction analysis shows that compound **5** crystallizes in the cubic system with the $Ia\bar{3}$ space group. Compound **5** consists of three L^2 molecules, three Cu^I ions, and two

halves of PMo_{12} anions (Figure 4a). There is only one kind of crystallographically unique Cu^I ion, which is two-coordinated in a linear geometry by two N atoms from two L^2 ligands. The bond distances and angles around the Cu^I ion are 1.78(1) Å, 1.82(1) Å, and 167.9(3)°.

In **5**, the L^2 molecules only exhibit a C-type conformation and act as a bidentate linker bridging Cu^I ions to form a 1D cationic chain (Figure S5, Supporting Information). Like in **3**, the Cu−O bond or the weak Cu−O bond interaction is absent in **5**. So the PMo_{12} anion just acts as a template, directing the $\{[Cu_3(L^2)_3]^{3+}\}_n$ coordination chains to array around it through hydrogen bonds. It may be caused by the stronger rigidity of the L^2 molecule, which prevents the PMo_{12} anion from approaching the Cu^I ion. Interestingly, six $\{[Cu_3(L^2)_3]^{3+}\}_n$ cationic chains form a cubic cage to host the PMo_{12} anion (Figure 4b). Furthermore, these cubic cages are stacked together to

Figure 4. (a) Ball-and-stick and polyhedron representations of the asymmetric unit of **5**, in which the hydrogen atoms are omitted for clarity. (b) Illustration of the environment of PMo_{12}. (c) View of the 3D stacking framework with two kinds of crystallographically unique PMo_{12} anions. Color code: a red ball denotes POM-1, turquoise denotes POM-2, a red chain means the vertical direction, a green chain is the horizontal direction, and a blue chain points perpendicular to the paper surface.

form a 3D supramolecular framework with two kinds of crystallographically unique PMo_{12} anions inserted into different layers, and then the whole structure is strengthened by the C−H···O hydrogen bonds (Figure 4c; for hydrogen bond distances and angles, see Table S2, Supporting Information).

Influence of Reaction Conditions on Compound Structures. In this work, our attention is focused on studying the effect of reaction conditions such as reactant species, reaction temperature, and the reactant molar ratio on constructing the POM-based coordination compounds.

Species. (i) Compounds **1** and **2** were synthesized under the same reaction conditions, except for using different POMs as building blocks. These two compounds are isostructual, which may be caused by PW_{12} (in **1**) and PMo_{12} (in **2**) being identical in charge, shape, and size. This result indicates that using PW_{12} or PMo_{12} as SBUs makes no difference on the products' structure under the same reaction conditions. (ii) Furthermore, we also assess the influence of the ligand length on the product structures. Compounds **4** and **5** were synthesized by using L^1 or L^2, respectively. In **4**, L^1 molecules adopt a Z-type or C/Z-type conformation, which coordinate with two crystallographically unique Cu^I ions to form a 1D chain. Meanwhile, the PW_{12} anions in **4** act as the bidentate linkers connecting these 1D coordination polymers into a 2D sheet structure. In comparison with L^1, the L^2 molecule

possesses longer rigid spacer. In **5**, L^2 molecules only display the C-type conformation, which coordinate with two crystallographically equivalent Cu^I ions to form a 1D chain. However, the PMo_{12} anions in **5** do not coordinate with any Cu^I ions. They just act as the templates to direct the $\{[Cu_3(L^2)_3]^{3+}\}_n$ coordination chains to array around them, then forming a hydrogen-bonding-stabilized 3D framework. This may be attributed to the L^2 molecule possessing a longer rigid spacer than L^1, which prevents the PMo_{12} anions from approaching $\{[Cu_3(L^2)_3]^{3+}\}_n$ moieties because of steric hindrance.

Temperature. Compounds **1** and **3** were synthesized under identical reaction conditions, except for the change of reaction temperature. Compound **1** was prepared at 150 °C, in which the Cu^I ions are three- or four-coordinated by L^1 ligands and PW_{12} anions. However, compound **3** was prepared at a relatively lower temperature (130 °C), in which the Cu^I ions are two- or three-coordinated by L^1 ligands. In addition, similar phenomena were found in the other three compounds; for example, the Cu^I ions are four- or three-coordinated in **2** (150 °C), three- or two-coordinated in **4** (130 °C), and two-coordinated in **5** (130 °C). According to our experimental results, it is supposed that a high reaction temperature is beneficial to increasing the coordination numbers of the Cu^I ions.

Molar Ratio. Compounds **3** and **4** were synthesized under the same reaction conditions, except for the
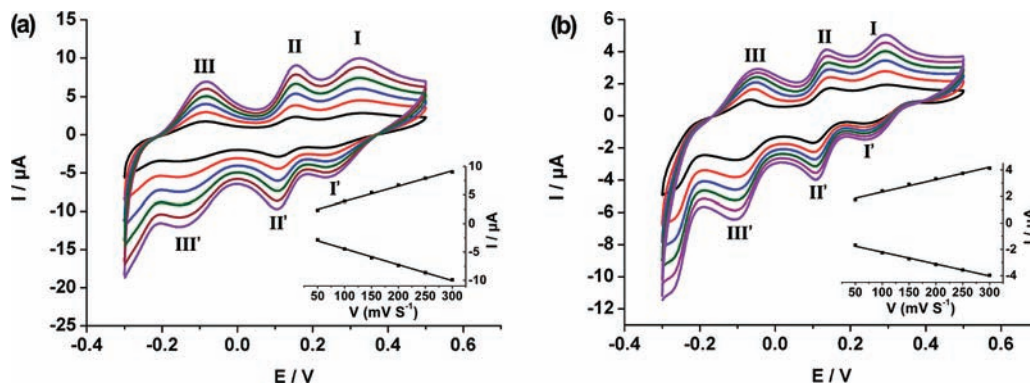
Figure 5. Cyclic voltammograms of (a) **2** and (b) **5** in 0.5 M H_2SO_4 under scan rates from inner to outer: 50, 100, 150, 200, 250, and 300 mV s^{-1}. The inserts show the relationship of the scan rates versus oxidation peak currents of Mo(II) and the reduction peak currents of Mo(II′).

reactant molar ratio. Compound **3** was synthesized with a reactant molar ratio of $Na_2WO_4/L^1/Cu(NO_3)_2 =$ 2:0.8:0.8 and was composed of one PW_{12} anion, four L^1 molecules, and three Cu^I ions. The L^1 ligand coordinated with the Cu^I ions to form a 2D network. However, when we reduced the molar ratio to $Na_2WO_4/L^1/Cu(NO_3)_2 =$ 2:0.4:0.4, we obtained compound **4** consisting of one PW_{12} anion, three L^1 molecules, and three Cu^I ions. Compared with **3**, **4** lost one L^1 molecule, leading to the formation of a 1D coordinated chain instead of a 2D sheet. Similar phenomena were also found in other compounds. For example, **1** and **2** were synthesized with the same reactant molar ratio as that for **3**, and they all possessed four ligands, while **5** was synthesized with the same reactant molar ratio as that for **4**, and they both possessed three ligands.

FT-IR, PXRD, and XPS Characterization. The IR spectra of compounds **1**−**5** are shown in Figure S6 in the Supporting Information. Characteristic bands at 1078, 964, 885, 816, and 758 cm^{-1} for **1**; 1079, 978, 891, 816, and 764 cm^{-1} for **3**; and 1080, 978, 893, 814, and 756 cm^{-1} for **4** are attributed to ν(P−O), ν(W=O), and ν(W−O−W), respectively. Bands in the regions of 1515−1275 cm^{-1} for **1**, 1519−1272 cm^{-1} for **3**, and 1519−1271 cm^{-1} for **4** are attributed to the L^1 ligand, respectively. In addition, characteristic bands at 1063, 958, 880, 808, and 754 cm^{-1} for **2** and 1061, 958, 879, 804, and 754 cm^{-1} for **5** are attributed to ν(P−O), ν(Mo=O), and ν(Mo−O−Mo), respectively. Bands in the regions of 1517−1280 cm^{-1} for **2** and 1633−1277 cm^{-1} for **5** are attributed to the L^1 and L^2 ligands, respectively.

The PXRD patterns for compounds **1**−**5** are presented in Figure S7, Supporting Information. The diffraction peaks of both calculated and experimental patterns match well, indicating the phase purities of these compounds.

The XPS spectra of compounds **1**−**5** are shown in Figure S8 in the Supporting Information. The XPS spectra show two peaks at 932.9 and 953.2 eV in **1**, 932.7 and 952.6 eV in **2**, 932.9 and 953.2 eV in **3**, 933.4 and 953.3 eV in **4**, and 933.2 and 953.0 eV in **5** attributed to $Cu^I(2p_{3/2})$ and $Cu^I(2p_{1/2})$. Two peaks at 36.2 and 37.8 eV in **1**, 36.4 and 38.0 eV in **3**, and 36.7 and 38.1 eV in **4** are ascribed to $W^{VI}(4f_{5/2})$ and $W^{VI}(4f_{7/2})$. Meanwhile, two peaks at 232.9 and 236.1 eV in **2** and 233.2 and 236.4 in **5** are ascribed to $Mo^{VI}(3d_{5/2})$ and $Mo^{VI}(3d_{3/2})$.

Electrochemical Characterization. Compounds **2** and **5** were decorated on the surface of the working electrode,

and then their redox properties were studied in a 0.5 M H_2SO_4 aqueous solution at room temperature. The electrochemical behaviors of the two compounds are similar except for some slight potential shift, as shown in Figure 5. In the potential range of −0.3 to +0.5 V, three pairs of redox peaks are observed, and their mean peak potentials $E_{1/2} = (E_{pa} + E_{pc})/2$ are 0.33, 0.16, and −0.08 V for **2** and 0.30, 0.14, and −0.07 V for **5**. These redox peaks should be ascribed to the three consecutive two-electron processes of Mo, indicating that the redox ability of the PMo_{12} anions are maintained in **2** and **5**.[22] With the increasing of scan rates from 50 to 300 mV s^{-1}, the anodic peak potentials are shifted slightly toward the positive direction, and the corresponding cathodic peak potentials are shifted slightly toward the negative direction, suggesting that the redox processes are surface-controlled.

It is well-known that POMs can be employed in electrocatalytic reduction for some acidic anions.[23] Herein, a simple and rapid method is used to study the electrocatalytic reduction behaviors of **2** and **5** for the $[IO_3]^-$ anion to confirm that the electrocatalytic activity of POMs is maintained in **2** and **5**. Experiment results illustrate that **2** and **5** perform good electrocatalytic activities for the reduction of the $[IO_3]^-$ anion in a 0.5 M H_2SO_4 aqueous solution. As shown in Figure 6, all of the reduction peak currents of the Mo atoms increase remarkably with the addition of $[IO_3]^-$, while the corresponding oxidation peak currents are decreased. These phenomena indicate that the three reductive species of the PMo_{12} anion in **2** and **5** all bear electrocatalytic activities for the reduction of the $[IO_3]^-$ anion.

(22) (a) Wang, P.; Yuan, Y.; Han, Z. B.; Zhu, G. Y. *J. Mater. Chem.* **2001**, *11*, 549–553. (b) Wang, P.; Wang, X. P.; Wang, X. Y; Zhu, G. Y. *Anal. Chim. Acta* **2000**, *424*, 51–56.

(23) (a) Nellutla, S.; Tol, J. V.; Dalal, N. S.; Bi, L. H.; Kortz, U.; Keita, B.; Nadjo, L.; Khitrov, G. A.; Marshall, A. G. *Inorg. Chem.* **2009**, *44*, 9795–9806. (b) Bi, L. H.; Kortz, U.; Nellutla, S.; Stowe, A. C.; Tol, J. V.; Dalal, N. S.; Keita, B.; Nadjo, L. *Inorg. Chem.* **2005**, *44*, 896–903. (c) Bi, L. H.; Shen, Y.; Jiang, J. G.; Wang, E. K.; Dong, S. J. *Anal. Chim. Acta* **2005**, *534*, 343–351. (d) Chen, L.; Tian, X. F.; Tian, L.; Liu, L.; Song, W. B.; Xu, H. D. *Anal. Bioanal. Chem.* **2005**, *382*, 1187–1195.

(24) The hysteresis phenomenon with increasing concentration of $[IO_3]^-$ during the electrocatalysis process may be caused by the slow response of the thin film to the reduction of a high concentration of $[IO_3]^-$. A similar result has been observed in the electrocatalysis of protein bearing film with a high concentration of nitrite. Nadjo et al. also reported a hysteresis phenomenon in the electrocatalysis for the reduction of nitrate in POM solution. Please see: (a) Fourmond, V.; Sabaty, M.; Arnoux, P.; Bertrand, P.; Pignol, D.; Léger, C. *J. Phys. Chem. B* **2010**, *114*, 3341–3347. (b) Keita, B.; Abdeljalil, E.; Nadjo, L.; Contant, R.; Belgiche, R. *Electrochem. Commun.* **2001**, *3*, 56–62.
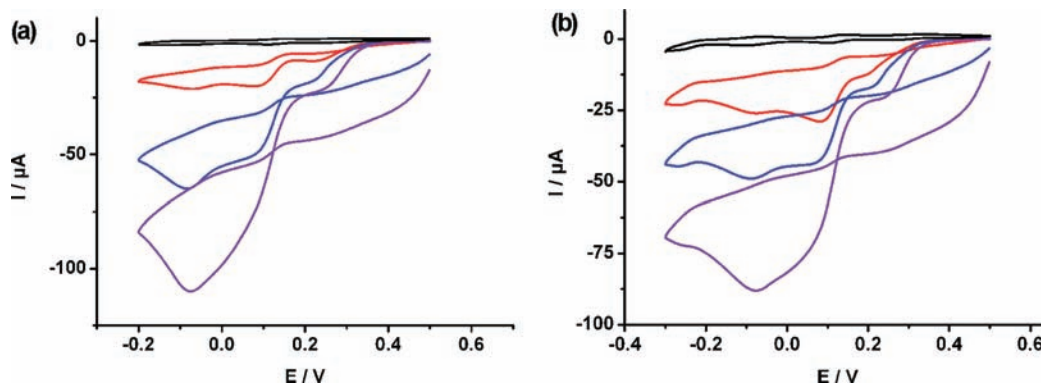
Figure 6. Cyclic voltammograms of (a) **2** and (b) **5** in a 0.5 M H_2SO_4 solution containing concentrations of $[IO_3]^-$. From top to bottom: 0, 5, 7.5, and 10 mM, under a scan rate of 50 mV s^{-1}.[24]
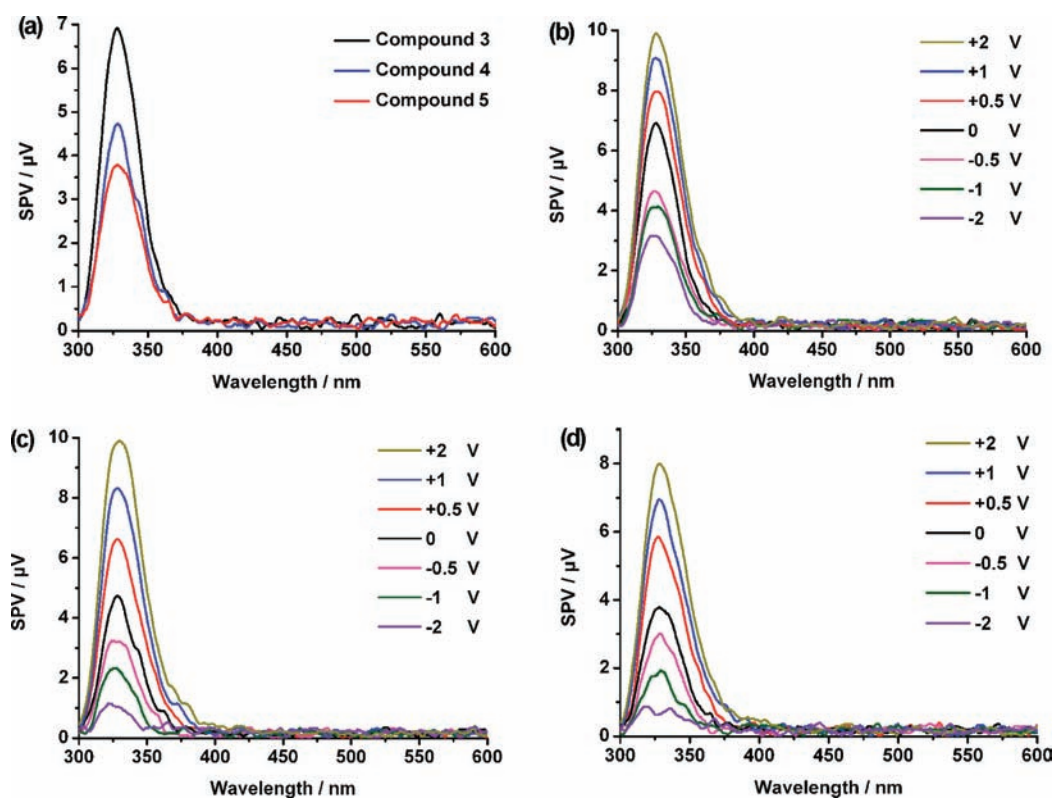
Figure 7. (a) SPS of compounds **3**−**5**. (b) EFISPS of **3**. (c) EFISPS of **4**. (d) EFISPS of **5**.

SPS and EFISPS Characterization. SPS and EFISPS are effective methods to investigate the processes of dye sensitization and photocatalysis and the photoelectric properties of a semiconductor.[25] However, to the best of our knowledge, the study of surface photovoltaic (SPV) behaviors of POM-containing materials is in its preliminary stage, with very limited publications relevant to the topic available.[5c,26] In this paper, we employed SPS and EFISPS to investigate the behaviors of photogenerated electrons and the photoelectric properties of compounds **3**−**5**. Such a characteristic indicates that these compounds can be used as potential photocatalytic framework materials for the degradation of organic molecules.

The curves of the SPS of compounds **3**−**5** show similar SPV response bands in the range of 300−375 nm (Figure 7a). The different intensities of the SPV may be caused by the different structures of the three compounds. For instance, **3** possesses a more regular network structure than **4** because the stacking fashion is the A−B type in **3** and the A−B−C type in **4**, which can supply more transmission passages for electrons or holes. More electrons

(25) (a) Lin, Y. H.; Wang, D. J.; Zhao, Q. D.; Yang, M.; Zhang, Q. L. *J. Phys. Chem. B* **2004**, *108*, 3202–3206. (b) Lenzmann, F.; Krueger, J.; Burnside, S.; Brooks, K.; Gratzel, M.; Gal, D.; Ruhle, S.; Cahen, D. *J. Phys. Chem. B* **2001**, *105*, 6347–6352. (c) Hou, X. K.; Du, X. G.; Ma, C. Y.; Li, Y.; Zhang, Q. L.; Wang, X.; Chang, Y, C.; Jiang, W. H.; Cheng, C. H.; Shan, S. J.; Du, G. T. *Synth. Met.* **2005**, *105*, 305–308. (d) Zhang, J.; Wang, D. J.; Shi, T. S.; Wang, B. H.; Sun, J. Z.; Li, T. J. *Thin Solid Films* **1996**, *596*, 284–286.

(26) (a) Li, S. Z.; Zhao, J. W.; Ma, P. T.; Du, J.; Niu, J. Y.; Wang, J. P. *Inorg. Chem.* **2009**, *48*, 9819–9830. (b) Li, M. X.; Liu, S. Z.; Zhang, C. M.; Du, Z. L.; Wong, W. Y. *Acta Chim. Sinica* **2005**, *63*, 1676–1680. (c) Liu, L.; Liu, Q.; Chen, M.; Li, M. J.; Xu, L. P.; Liu, S. Z.; Du, Z. L.; Wong, W. Y. *Aust. J. Chem.* **2010**, *63*, 103–108. (d) Liu, L.; Zhang, G. S.; Liu, S. Z.; Ai, W. H.; Zhang, C. M.; Du, Z. L.; Wong, W. Y. *Acta Chim. Sinica* **2005**, *63*, 2194–2198.

diffusing to the surface can lead to an increase of SPV intensity.[27] So the SPV intensity of **3** is higher than that of **4**. Nevertheless, **5** possesses the lowest regular hydrogen bonding structure in these three compounds; hence, it shows the lowest SPV intensity.

The EFISPSs of compounds **3**−**5** are shown in Figure 7b−d. The EFISPS results show that similar SPV responses for **3**−**5** under the external electric fields changed from −2 to +2 V. The SPV response intensities of these three compounds all increase when the positive fields increase, while they reduce when the external negative fields increase. This is attributed to the positive electric field being beneficial to the separation of photo-excited electron−hole pairs, which in turn results in an increase of response intensity; however, the negative electric field has just the opposite effect, suggesting that **3**−**5** possess the *n*-type semiconductor characteristic.[5c,26a,28]

Conclusions

Five Keggin POM-based inorganic−organic hybrid compounds, **1**−**5**, have been synthesized and characterized, and their structural relationships with the reaction conditions have also been studied. Research results indicate that the assembly of POMs and flexible ligand L^1 and L^2 coordination compounds can be controlled by tuning the reaction conditions. (i) Compounds **1** and **2** were synthesized at 150 °C, in which the Cu^I ions are three-coordinated or four-coordinated, while compounds **3**−**5** were synthesized at 130 °C, in which the Cu^I ions are two-coordinated or three-coordinated. It is supposed that the reaction temperature may affect the coordination number of Cu ions; that is, a high reaction temperature is beneficial to increasing the coordination ability of center Cu^I ions. (ii) Compounds **4** and **5** were synthesized with a relatively lower reactant molar ratio in

comparison with that for the synthesis of **1**−**3**, in which the cationic coordination moieties all present 1D chain structures in contrast to the 2D sheets in **1**−**3**, indicating that the reactant molar ratio may result in different arrangements of coordination moieties; that is, a high reactant molar ratio of the ligand and $Cu(NO_3)_2$ to molybdates/tungstates tends to increase the dimensions of [CuL] coordination polymers. (iii) Compound **5** was synthesized by using the L^2 ligand instead of L^1 for **1**−**4**, in which the $\{[Cu_3(L^2)_3]^{3+}\}_n$ moieties exhibit larger steric hindrance to coordinate with POM building blocks than $\{[Cu_3(L^1)_3]^{3+}\}_n$ and $\{[Cu_3(L^1)_4]^{3+}\}_n$ moieties in **1**−**4**, suggesting that longer ligands possess larger steric hindrance, which is bad for the coordination of POMs with [CuL] moieties. In summary, this work provides useful information for the design and synthesis of POM-based coordination compounds. Further work is in progress to evaluate the influence of the charge number of POMs on the preparation of coordination macrocycles based on [CuL¹] moieties. The electrocatalytic properties of **2** and **5** and the SPS responses of **3**−**5** suggest that these compounds can be used as potential electrocatalytic or photocatalytic framework materials. In addition, EFISPS curves indicate that **3**−**5** possess the *n*-type semiconductor characteristic.

Supporting Information Available: X-ray crystallographic files in CIF format; table of selected bond lengths and bond angles; FT-IR, PXRD and XPS spectra; and structure figures in PDF format. This material is available free of charge via the Internet at http://pubs.acs.org.

(27) Zhang, L.; Niu, S. Y.; Jin, J.; Sun, L. P.; Yang, G. D.; Ye, L. *Inorg. Chim. Acta* **2009**, *362*, 1448–1454.
(28) He, T.; Yao, J. N. *J. Mater. Chem.* **2007**, *17*, 4547–4557.